

pubs.acs.org/cm Article

Red-to-Blue Photon Upconversion Enabled by One-Dimensional CdTe Nanorods

Zachary A. VanOrman, Carl R. Conti, III, Geoffrey F. Strouse, and Lea Nienhaus*



Cite This: *Chem. Mater.* 2021, 33, 452–458



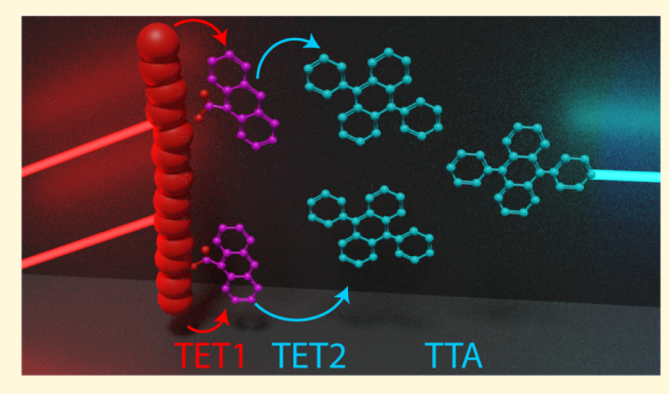
ACCESS

Metrics & More



Supporting Information

ABSTRACT: Photon upconversion via triplet—triplet annihilation creating light in the high-energy regime of the visible spectrum could prove particularly useful in applications such as photocatalysis. Quantum-confined semiconductor nanocrystals have previously been shown to function as efficient triplet sensitizers in green-to-blue upconversion schemes, but an improvement in the apparent anti-Stokes shift of the upconversion scheme will be beneficial for future commercial applications. Additionally, both zero- and two-dimensional quantum-confined sensitizers have been investigated but not one-dimensional nanomaterials. In this work, we fill a hole in the present field of photon upconversion by accomplishing both of these feats. Specifically, we introduce CdTe nanorods as a new class of triplet sensitizers for red-to-blue photon upconversion. When the triplet transmitter ligand (9-anthracene-



carboxylic acid) and triplet annihilator (9,10-diphenylanthracene) are added to the nanorods, we observe efficient photon upconversion at a normalized upconversion efficiency of $\eta_{\rm uc} = 4.3\%$ and a low threshold power of $I_{\rm th} = 93$ mW/cm². The introduction of one-dimensional triplet sensitizers could yield future research that effectively harnesses the unique properties of these materials, allowing for new approaches for efficient photon upconversion, especially at large apparent anti-Stokes shifts.

■ INTRODUCTION

Photon upconversion (UC) via triplet—triplet annihilation (TTA) in organic semiconductors is an efficient way to generate higher energy photons at relatively low fluences. TTA-UC could prove to be useful in a multitude of applications, such as photocatalysis, optogenetics, photovoltaics, or bioimaging. In lieu of metal—organic complexes with exchange energy losses on the order of hundreds of meVs, recently, inorganic semiconductor materials including bulk perovskites and spherical semiconductor quantum dots (QDs) have emerged as efficient triplet sensitizers for the TTA-UC process.

Additionally, quantum-confined semiconductor materials beyond QDs have been studied, namely, two-dimensional (2D) nanoplatelets (NPLs), as these materials are less prone to parasitic effects stemming from size polydispersity. However, one-dimensional (1D) materials, where two dimensions of the nanomaterial are quantum-confined, have not yet been investigated as potential triplet sensitizers. Here, we introduce cadmium telluride (CdTe) nanorods (NRs) as triplet sensitizers for anthracene-based upconverters.

1D nanomaterials, such as NRs, and nanowires, have been previously studied for a multitude of applications, including lasing, ¹⁸ photonics, ¹⁹ bioelectronics, ²⁰ and photovoltaics. ²¹ The well-defined facets and unique anisotropic shape of 1D nanomaterials also allow for self-assembly into macro-

structures,²² which could be useful for photon UC, especially in the solid state.^{23,24} In-depth studies of the unique properties of 1D materials endowed by their aspect ratio and anisotropic nature are required pertaining to their application as triplet sensitizers in photon UC via TTA.

These NRs not only fill in a gap of the material dimensionality of existing triplet sensitizers but also in the energetic regime of UC under study. While green-to-blue 14,25,26 and blue-to-UV UC schemes 27-29 are useful for photocatalytic applications, it could also be beneficial to extend the apparent anti-Stokes shift of the TTA-UC system, yielding a system capable of red-to-blue UC or beyond.

Recent works have realized red-to-blue UC using silicon QDs³⁰ and cadmium selenide (CdSe) QDs as triplet sensitizers.³¹ However, silicon QDs exhibit relatively low photoluminescent quantum yields (QYs), and red-emitting CdSe QDs are on the edge of the quantum confinement regime, which has been shown to have negative impacts on the

Received: November 19, 2020 Revised: December 16, 2020 Published: December 29, 2020





efficiency of the UC process.^{26,32,33} We take advantage of CdTe, which allows for redder emission at smaller nanocrystal sizes as compared to CdSe.³⁴ The as-synthesized NRs can be paired with a transmitter ligand and a triplet annihilator to realize efficient red-to-blue UC. We use 9-anthracene carboxylic acid (ACA) as the triplet transmitter ligand and 9,10-diphenylanthracene (DPA) as the blue-emitting triplet annihilator. ACA has previously been used as a transmitter ligand for CdSe QD-sensitized UC schemes, ^{14,26} where the triplet energy transfer (TET) process has been shown to occur through space.³⁵

Here, we observe efficient red-to-blue TTA-UC with UC efficiencies in excess of 4% with an apparent anti-Stokes shift of 0.82 eV. Additionally, we observe a power threshold for an efficient UC of $I_{\rm th} = 93$ mW/cm², which is considerably lower than the majority of systems utilizing quantum-confined triplet sensitizers. ^{17,25,31,36} Most importantly, we open the door to a new frontier of triplet sensitizer materials in the form of 1D semiconductor nanocrystals.

■ RESULTS/DISCUSSION

CdTe NRs were synthesized by injecting 36 mg of Te in 3 mL of trioctylphosphine (TOP) into a Cd-oleate solution at 200 °C (see Experimental Methods). Upon purification with acetone and methanol, the NRs were resuspended in hexanes. As shown in the scanning transmission electron microscopy (STEM) image in Figure 1a, the NRs are slightly curved in

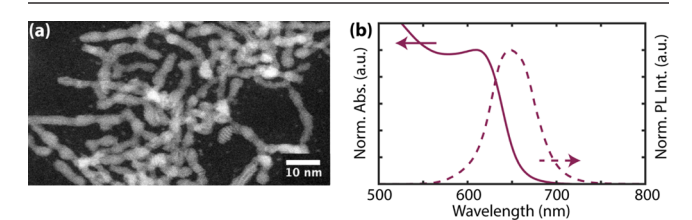


Figure 1. CdTe NR characterization. (a) STEM image of the CdTe NRs. (b) Normalized absorbance and PL emission of the CdTe NRs. The PL emission of the NRs was monitored under 520 nm excitation, where a 550 nm long-pass filter was used to remove excess laser scatter.

appearance with a radius of \sim 3 nm. Additional high-resolution STEM images are shown in Figure S1. Figure 1b shows the normalized absorbance and photoluminescence (PL) spectrum of the NRs in hexanes, where the emission peak maximum is at 649 nm, slightly Stokes-shifted from the maximum absorbance of \sim 612 nm.

Additionally, we note that the appearance of the emission peak changes upon stirring the NRs vigorously overnight. While the absorption spectrum does not change in the stirred NRs, the emission peak maximum blue-shifts to ~633 nm (Figure S2). We attribute this to resonance energy transfer between aggregated NRs, where the blue edge of the emission spectrum appears to be quenched in the unstirred sample. ^{37,38}

In order to obtain efficient red-to-blue TTA-UC, in addition to the triplet sensitizer, both a triplet mediator or transmitter ligand and a triplet annihilator are required. The overall energetic scheme of the TTA-UC system is shown in Figure 2a. Upon optical excitation via absorption of an incident photon, an electron is excited from the valence band to the conduction band in the CdTe NR. The spin-triplet state of the ACA transmitter ligand can then be populated via a TET

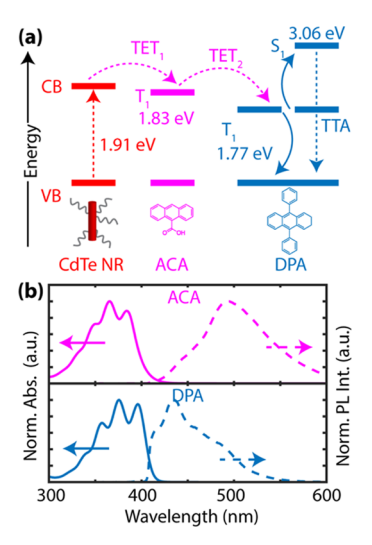


Figure 2. Proposed CdTe NR-sensitized UC system. (a) Schematic of the energy levels involved in the UC process, including the CdTe NR sensitizer band gap (red), ACA triplet energy level (magenta), and DPA triplet- and singlet-state energies (blue). (b) Normalized absorbance (solid) and PL emission (dashed) of ACA (top, magenta) and DPA (bottom, blue).

following a Dexter-type exchange mechanism, 40 which is energetically favorable in this case, as the NR excitonic transition is higher in energy than the ACA triplet level T_1 = 1.83 eV. 14 A second TET (TET₂) can then occur to DPA, which has a T₁ energy level of 1.77 eV. Once two DPA triplet states are occupied, and the two triplet-excited molecules collide, TTA-UC can occur. Upon relaxation of the resultant singlet excited state, a blue photon is emitted correlated to the S₁ energy level of DPA at 3.06 eV. The normalized absorbance and PL emission spectra for the relevant transmitter ligand, ACA, and triplet annihilator, DPA, are shown in Figure 2b. The UC emission of the ternary NR-ACA-DPA UC system will manifest as emission from the DPA after the TTA-UC process has occurred. Therefore, taken from the absorbance maximum of the sensitizer and the emission maximum of the annihilator, the apparent anti-Stokes shift of the system presented here is 0.82 eV,41 which is comparable to recently reported red-to-blue QD-sensitized UC schemes. 31,42

The ligand exchange process occurs through the addition of ACA in chlorobenzene and allowing the solutions to stir overnight. This process not only helps to promote a dynamic ligand exchange environment between the oleate-capped NRs and the ACA but also helps to suppress the aggregation of the NRs discussed previously.

Here, we utilize a combination of ultrafast transient absorption (TA) and time-resolved PL spectroscopy in the form of time-correlated single-photon counting (TCSPC) to unravel the energy transfer process between the NRs and surface-bound ACA. The TA spectrum of NRs with their native ligand shell is shown in Figure 3a, where four distinct features are shown, corresponding to excitonic transitions at different energies. Most notable is the ground-state exciton bleach (XB) at 635 nm because of state filling in the NRs. Additionally, two photoinduced absorption (PIA) features can be discerned at 550 and 487 nm, where PIA features arise because of shifts in excited-state energy levels. An additional bleach can be found at 435 nm. To observe the change in the NR TA features after ligand exchange with ACA, the ultrafast

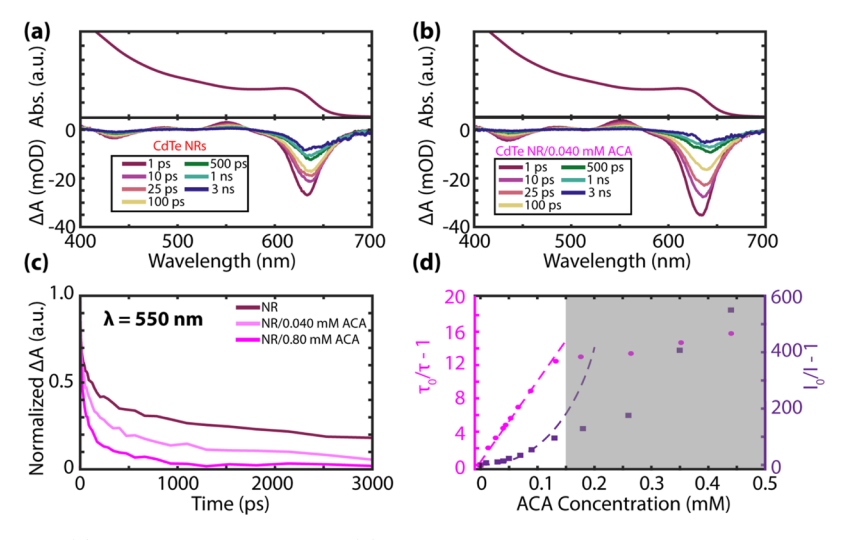


Figure 3. Ultrafast TA spectra of (a) the native CdTe NRs and (b) NRs with 0.040 mM ACA at various delay times after excitation at the band edge (625 nm). (c) TA kinetics of the PIA peak at 550 nm for the NR-only (red), NR with 0.040 mM ACA (light magenta) and 0.80 mM ACA (magenta). (d) Stern-Volmer plots of the NR lifetime (magenta, circles) and the steady-state emission intensity (purple, squares). The gray region denotes an apparent saturation point of the quenching.

TA measurements were repeated under the same conditions for the NR-ACA system (Figure 3b). Additionally, a sample with a concentration of ACA 20 times higher is shown in Figure S3a. Other studies have shown that upon triplet sensitization of ACA, an excited-state absorption (ESA) feature centered at ~435 nm can be observed upon excitation of the QD, corresponding to the ACA $T_1 - T_n$ transition. 35,42,45 However, this is not observed in Figure 3b as the high-energy NR bleach feature is also centered at 435 nm, which obscures the ACA ESA peak. Additionally, the kinetics of the PIA feature at 550 nm are shown in Figure 3c, where the PIA lifetime is quenched upon the addition of ACA. Furthermore, the kinetics of the PIA feature at 487 nm, as well as the two bleach features, the XB at 635 nm, and the high-energy bleach feature at 435 nm are shown in Figure S3, where the same trend is observed, that is, the lifetime is shortened upon a higher concentration of the ACA transmitter ligand. We emphasize that the XB kinetics are convoluted by the pump signal (625 nm) and that the bleach at 435 nm contains contributions from the ACA ESA.

The effect of the ACA coupling on the NR in both steady-state and time-resolved emission was also monitored. Figure S4 shows the effect of the time-resolved emission, monitored via TCSPC, and the steady-state emission of the NR upon addition of ACA. In both cases, the emission is significantly quenched. As the lifetimes measured here are multiexponential in nature, we take the PL lifetime, τ as the point at which the normalized PL emission has decayed to 1/e. To further describe the degree of quenching of the NR emission, we plot in Figure 3d, both the quenching of the PL lifetime (τ_0/τ) and of the steady-state emission (I_0/I) , in accordance with the Stern–Volmer equation given in eq 1.

$$\frac{\tau_0}{\tau} = 1 + K_{SV}[Q] \tag{1}$$

 $K_{\rm SV}$ corresponds to the Stern–Volmer constant, which is the product of the bimolecular quenching constant $k_{\rm q}$ and the native lifetime τ_0 , and [Q] is the concentration of the quenching species, which, here, is the concentration of ACA. We observe a linear behavior from the quenching of the lifetime and a quadratic behavior for the quenching of the

steady-state emission, which indicates the presence of both static and dynamic quenching, in line with similar behavior observed in 0D CdSe QDs and 2D CdSe NPLs. ¹⁷ From the Stern–Volmer plot (with concentrations <0.10 mM ACA), we extract a bimolecular quenching constant of 8.82×10^{12} M⁻¹ s⁻¹ (see Supporting Information for more information). Above a concentration of ~0.15 mM ACA, a saturation of the quenching is observed, which is highlighted in Figure 3d by a gray box.

The addition of DPA to NRs coupled with ACA results in a ternary system capable of TTA-UC, which can easily be observed by eye, as shown by the photographs in Figure 4a. When there is no ACA, little UC can be observed, and a cuvette containing NRs and DPA emits mostly red light upon 520 nm excitation because of emission from the NRs. However, if the NRs are complexed with ACA before the

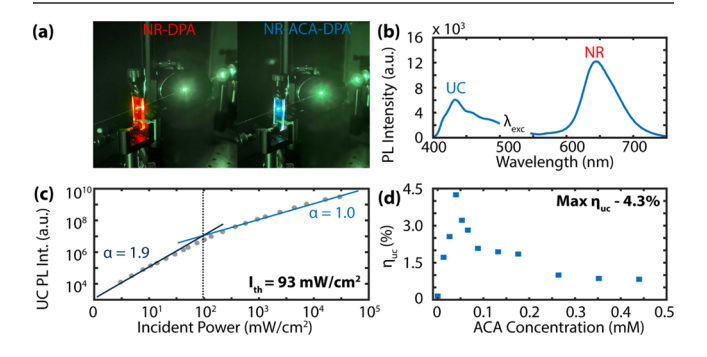


Figure 4. Characterization of the CdTe NR-sensitized UC process. (a) Photograph of the NR-DPA system (left) without ACA and the NR-ACA-DPA UC system (right), where the blue emission can be observed as a result of TTA-UC. (b) Steady-state emission of the NR-ACA-DPA system under 520 nm excitation. The region from 500 to 540 nm was removed because of excess laser scatter. (c) Log–log plot of the UC PL intensity against the incident power applied to the NR-ACA-DPA UC system with 0.04 mM ACA yielding an $I_{\rm th}=93$ mW/cm². (d) UC efficiency, $\eta_{\rm uc}$ plotted as a function of the added ACA concentration. The maximum $\eta_{\rm uc}=4.3\%$ is observed at a concentration of 0.04 mM ACA.

DPA is added, blue emission from the S_1 state of DPA can be observed.

The emission spectrum of the NR-ACA-DPA system is shown in Figure 4b, where the 520 nm excitation results in emission not only from the NR but also from the DPA annihilator. The region from ~500 to 540 nm was removed from the PL spectrum because of laser scatter. The UC emission spectrum matches that which is observed upon direct excitation of DPA at 405 nm, as shown in Figure 2b. The intensity of the upconverted emission follows a power dependence characteristic of TTA-UC systems, which is shown in a log-log plot of the UC PL intensity against the incident power in Figure 4c. At low powers, the upconverted PL increases quadratically with the incident power. This is the regime where triplet decay pathways other than TTA are dominant, which yields a slope $\alpha = 2$ in a log-log plot.⁴⁶ At high powers, where TTA is the dominant triplet decay pathway, the upconverted PL increases linearly with the incident power, yielding $\alpha = 1$. This behavior characteristic of TTA-UC stems from the coupled rate equations of the UC system, which has been discussed at length elsewhere. 46-49

The point at which these regimes meet gives the threshold intensity value $I_{\rm th}$, which is a figure of merit for the power density at which the TTA-UC process becomes efficient. For the system with the most efficient TTA-UC, at an added concentration of 0.04 mM ACA, an $I_{\rm th}$ value of 93 mW/cm² was determined, which is considerably lower compared to many other quantum confined semiconductor-sensitized systems, $^{12,17,25,28,29,36,50}_{12,17,25,28,29,36,50}$ especially those that exhibit red-to-blue UC. $^{31,42}_{12,11,12}$ Only the upconverted emission follows this unique power dependence, and the excitonic NR emission exhibits the expected linear regime at all powers, as shown in Figure S5.

Additionally, the UC efficiency, notated as $\eta_{\rm uc}$, was measured relative to a rubrene standard for different ACA concentrations, which is shown in Figure 4d. Here, we choose to normalize the UC QY by two, as TTA is a two-photon to one process, meaning the upper limit of the UC QY is 50%. If $\eta_{\rm uc}$ was calculated according to Castellano and co-workers, where the absorbance and UC emission of the NR-ACA-DPA system was compared to that of rubrene, which is shown in Figure S6, in accordance with eq 2.

$$\eta_{\rm uc} = 2 \frac{\Phi_{\rm rub}}{\Phi_{\rm DPA}} \left(\frac{A_{\rm rub}}{A_{\rm UC}} \right) \left(\frac{I_{\rm UC}}{I_{\rm rub}} \right) \left(\frac{n_{\rm UC}}{n_{\rm rub}} \right)^2 \tag{2}$$

 $\Phi_{\rm rub}$ is the PLQY of rubrene, which is divided by the QY of DPA, as the annihilator QY is not at unity, A reflects the absorption of either the rubrene standard or the UC system at the excitation wavelength of 520 nm, I is the integrated emission spectrum, and n corresponds to the refractive index of either system (for more detail, see Supporting Information). Only faint UC is observed without the presence of ACA, and the $\eta_{\rm uc}$ increases to a maximum of $\eta_{\rm uc} = 4.3\%$ at an optimal added ACA concentration of 0.04 mM and then decreases sharply (compare Table S1).

As expected, we observe that the ACA ligand concentrations which result in higher $\eta_{\rm uc}$ values also yield lower $I_{\rm th}$ values, as shown in Figure S5. Both the NR-DPA system and a NR-ACA-DPA UC system with an ACA concentration much higher than the optimal concentration have $I_{\rm th}$ values near 1 W/cm², nearly ten times higher than that of the optimal concentration of 0.04 mM. At concentrations closer to the optimal concentration of

0.04 mM (Figure S5d), the $I_{\rm th}$ begins to decrease toward the lowest $I_{\rm th}$ of 93 mW/cm². While it is simpler to imagine the lower $\eta_{\rm uc}$ stemming from less bound ACA, that is, concentrations below 0.04 mM, the decline of $\eta_{\rm uc}$ above the optimal ACA concentration has also been previously observed in CdSe QD-sensitized systems. 42,50,51

The cause of this decline in the $\eta_{\rm uc}$ above the optimal concentration has not yet been completely unraveled in the previously reported QD-sensitized systems and cannot yet be attributed to a certain process in the NR-sensitized UC presented here and will be the focus of further investigations. For example, the role of the internal grain boundaries where nanoparticles were fused to obtain the elongated NRs in the UC mechanism is unclear and is of future interest. It is possible that these act as undesired recombination centers and thus result in a decrease of the possible UC efficiency. In addition, in the UC system presented here, the likelihood of aggregation of the 1D NRs introduces another potential loss pathway analogous to NPL stacking, which has been observed previously in NPL-sensitized TTA-UC. 17

In conclusion, we have shown that CdTe NRs are viable triplet sensitizers for use in red-to-blue UC schemes, which is specifically reflected by the $\eta_{\rm uc}$ exceeding 4% and the $I_{\rm th}$ value below 100 mW/cm² at an optimal ACA concentration of 0.04 mM. Additionally, this work fills a current gap in literature by introducing 1D triplet sensitizers for TTA-UC, which represent a new avenue for triplet sensitizer design in TTA-UC. The rich knowledge of 1D semiconductor nanomaterials gleaned from other applications applied to the field of photon UC could allow for new frontiers to be uncovered. For example, directed emission and ordered self-assembly could prove to be useful directions of research to create novel TTA-UC devices. Furthermore, we demonstrate that CdTe can act as an efficient material for triplet sensitization as it has not yet been explored in depth.⁵² Beyond the scope of the work presented here, further investigation of the loss mechanisms occurring at higher ACA concentrations will allow for a better understanding of the energy transfer processes, which can translate into even higher UC efficiencies, pushing TTA-UC toward its eventual industrial relevance.

EXPERIMENTAL METHODS

Materials. Tellurium (30 mesh), TOP, cadmium oxide, oleic acid, octadecene, methanol, hexanes, chlorobenzene, toluene, and rubrene were purchased from Millipore Sigma. ACA and DPA were purchased from TCI Chemicals. Acetone was purchased from Fisher. All chemicals were used as received without further modification.

Te-TOP Preparation. Te-TOP solution was made by adding 36 mg of Te powder to 3 mL of TOP. The mixture was lightly heated at 35 $^{\circ}$ C and stirred for 1 h in a glovebox under air-free conditions.

CdTe NR Synthesis. CdTe NRs were synthesized by first adding 120 mg of CdO, 1.33 mL of oleic acid, and 15 mL of octadecene into a 25 mL three-neck flask. The mixture was degassed under vacuum at 120 °C for 1 h. The mixture was then put under $\rm N_2$ gas and brought to 200 °C. After the solution became clear, 3 mL of Te-TOP was injected quickly. The reaction mixture was maintained at 200 °C for 5 min and then was allowed to cool in air. The NRs were quickly transferred to a $\rm N_2$ atmosphere glovebox for purification.

CdTe NR Purification. A total of 15 mL of a mixture of acetone and methanol were added to the NR solution before centrifugation at 6000 rpm for 15 min. The pellet was then redispersed in 1 mL hexanes.

Ligand Exchange. From the 1 mL hexane-concentrated NR solution, 50 μ L was diluted to 12 mL to make a NR stock solution. Various amounts of ACA and chlorobenzene were added to 200 μ L of

the NR stock solution, and the ACA in chlorobenzene was 3.08 mM. In all cases, the NR concentration and the amount of chlorobenzene added was kept constant. Following ligand exchange, no further purification was attempted to maintain a maximal QY of the NRs and maintain high binding fraction of the ACA because of the dynamic ligand binding occurring.

UC Sample Preparation. For UC measurements, 150 μ L of a 10 mg/mL DPA in chlorobenzene was added to 200 μ L of NR-ACA solution. The samples were prepared in the glovebox, and the 1 mm path-length cuvettes were sealed with electrical tape.

METHODS

Transmission Electron Microscopy. STEM images were measured by using a JEOL-JEM ARM200cF microscope.

Steady-State Optical Characterization. UV—visible absorption spectra were measured by a Thermo Scientific Evolution 220 spectrophotometer. Steady-state emission spectra were monitored via an Ocean Optics spectrometer (HR2000+ES) under either 405 nm continuous wave (CW) (LDH-D-C-405, PicoQuant) or 520 nm CW (LDH-D-C-520, PicoQuant) excitation. In the case of 405 nm excitation, excess laser scatter was removed by a 425 nm long pass filter (ThorLabs). For NR-only steady-state emission, excess laser scatter was removed via a 550 nm long pass filter (ThorLabs). For UC steady-state emission spectra, no filter was used to monitor both the NR and UC emission.

Ultrafast Transient Absorption. TA was performed using a HELIOS Fire transient absorption spectrometer (Ultrafast Systems). Femtosecond pulses were generated using a Coherent Astrella-V-F-1K amplifier system. A Vitara-S Coherent Ti:sapphire laser was amplified using a 1 kHz Coherent Revolution-50 pump laser and generated a 5 mJ pulse with a 100 fs full width half maximum at 800 nm. The pulse was split into a pump and a probe beam, where the probe was directed through a delay stage, while the pump passed through an optical parametric amplifier (OPerA Solo, Coherent). The white light continuum used for the probe was produced by a CaF2 crystal for all measurements. The pump and probe beam were then overlapped on the solution sample, which was previously sealed in a 1 mm path length UV quartz cuvette (Starna Cells) inside of an inert atmosphere glovebox. Difference spectra and single wavelength kinetics were collected averaging 3 times and holding for 3 s, with an exponential point acquisition beginning with 0.01 ps steps and totaling to 100 points. Data were processed using the Surface Xplorer software package from Ultrafast Systems.

Time-Correlated Single Photon Counting. PL lifetimes were collected by TCPSC, as detailed previously. ^{11,17,53} Lifetimes were measured under 520 nm excitation at a repetition frequency of 1 MHz. Photon arrival times were histogrammed by a MultiHarp 150 (PicoQuant) at a single photon counting avalanche diode (Micron Photon Devices). All lifetimes were measured at a power of 15 mJ. I_{th} measurements were conducted under similar conditions; however, the 520 nm laser was operated at CW and a 500 nm short pass filter (ThorLabs) was applied to remove laser scatter and the NR emission.

ASSOCIATED CONTENT

Supporting Information

The Supporting Information is available free of charge at https://pubs.acs.org/doi/10.1021/acs.chemmater.0c04468.

Stern–Volmer quenching calculation information, UC efficiency calculations, and supplemental figures: tabulated lifetimes and $\eta_{\rm uc}$ for CdTe NRs with various concentrations of ACA; additional high-resolution STEM images; UV–visible absorption and PL emission spectra of stirred and unstirred CdTe NRs; ultrafast TA spectrum of a NR-0.80 mM ACA solution at various delay times along with other kinetic decay traces from various features in the TA spectra; NR time-resolved and steady-state PL emission quenching upon addition of

ACA; $I_{\rm th}$ plots of the NR only emission along with UC $I_{\rm th}$ plots with various ACA concentrations; UV-vis absorption and PL emission of the rubrene standard (PDF)

AUTHOR INFORMATION

Corresponding Author

Lea Nienhaus — Department of Chemistry and Biochemistry, Florida State University, Tallahassee, Florida 32306, United States; orcid.org/0000-0003-1412-412X; Email: lnienhaus@fsu.edu

Authors

Zachary A. VanOrman – Department of Chemistry and Biochemistry, Florida State University, Tallahassee, Florida 32306. United States

Carl R. Conti, III – Department of Chemistry and Biochemistry, Florida State University, Tallahassee, Florida 32306, United States

Geoffrey F. Strouse – Department of Chemistry and Biochemistry, Florida State University, Tallahassee, Florida 32306, United States; orcid.org/0000-0003-0841-282X

Complete contact information is available at: https://pubs.acs.org/10.1021/acs.chemmater.0c04468

Notes

The authors declare no competing financial interest.

ACKNOWLEDGMENTS

Z.A.V. and L.N. acknowledge Florida State University startup funds and a planning grant from the Council on Research and Creativity (CRC) at FSU. C.R.C. and G.F.S. acknowledge the National Science Foundation under grant no. DMR-1905757. We thank Yan Xin for STEM measurements. A portion of this work was performed at the National High Magnetic Field Laboratory, which is supported by the National Science Foundation Cooperative agreement no. DMR-1644779 and the State of Florida. Transient absorption measurements were performed on a spectrometer supported by the National Science Foundation under grant no. CHE-1919633.

REFERENCES

- (1) Singh-Rachford, T. N.; Castellano, F. N. Photon Upconversion Based on Sensitized Triplet–Triplet Annihilation. *Coord. Chem. Rev.* **2010**, 254, 2560–2573.
- (2) Khnayzer, R. S.; Blumhoff, J.; Harrington, J. A.; Haefele, A.; Deng, F.; Castellano, F. N. Upconversion-Powered Photoelectrochemistry. *Chem. Commun.* **2011**, *48*, 209–211.
- (3) Ravetz, B. D.; Pun, A. B.; Churchill, E. M.; Congreve, D. N.; Rovis, T.; Campos, L. M. Photoredox Catalysis Using Infrared Light via Triplet Fusion Upconversion. *Nature* **2019**, *565*, 343.
- (4) Pfund, B.; Steffen, D. M.; Schreier, M. R.; Bertrams, M.-S.; Ye, C.; Börjesson, K.; Wenger, O. S.; Kerzig, C. UV Light Generation and Challenging Photoreactions Enabled by Upconversion in Water. *J. Am. Chem. Soc.* **2020**, *142*, 10468–10476.
- (5) Sasaki, Y.; Oshikawa, M.; Bharmoria, P.; Kouno, H.; Hayashi-Takagi, A.; Sato, M.; Ajioka, I.; Yanai, N.; Kimizuka, N. Near-Infrared Optogenetic Genome Engineering Based on Photon-Upconversion Hydrogels. *Angew. Chem., Int. Ed.* **2019**, *58*, 17827–17833.
- (6) Schulze, T. F.; Schmidt, T. W. Photochemical Upconversion: Present Status and Prospects for Its Application to Solar Energy Conversion. *Energy Environ. Sci.* **2014**, *8*, 103–125.

- (7) Ferreira, R. A. S.; Correia, S. F. H.; Monguzzi, A.; Liu, X.; Meinardi, F. Spectral Converters for Photovoltaics—What's Ahead. *Mater. Today* **2020**, 33, 105–121.
- (8) Askes, S. H. C.; Pomp, W.; Hopkins, S. L.; Kros, A.; Wu, S.; Schmidt, T.; Bonnet, S. Imaging Upconverting Polymersomes in Cancer Cells: Biocompatible Antioxidants Brighten Triplet—Triplet Annihilation Upconversion. *Small* **2016**, *12*, 5579—5590.
- (9) Amemori, S.; Sasaki, Y.; Yanai, N.; Kimizuka, N. Near-Infrared-to-Visible Photon Upconversion Sensitized by a Metal Complex with Spin-Forbidden yet Strong S0-T1 Absorption. *J. Am. Chem. Soc.* **2016**, 138, 8702–8705.
- (10) Nienhaus, L.; Correa-Baena, J.-P.; Wieghold, S.; Einzinger, M.; Lin, T.-A.; Shulenberger, K. E.; Klein, N. D.; Wu, M.; Bulović, V.; Buonassisi, T.; Baldo, M. A.; Bawendi, M. G. Triplet-Sensitization by Lead Halide Perovskite Thin Films for near-Infrared-to-Visible Upconversion. ACS Energy Lett. 2019, 4, 888–895.
- (11) Wieghold, S.; Bieber, A. S.; VanOrman, Z. A.; Daley, L.; Leger, M.; Correa-Baena, J.-P.; Nienhaus, L. Triplet Sensitization by Lead Halide Perovskite Thin Films for Efficient Solid-State Photon Upconversion at Subsolar Fluxes. *Matter* **2019**, *1*, 705–719.
- (12) VanOrman, Z. A.; Bieber, A. S.; Wieghold, S.; Nienhaus, L. A Perspective on Triplet Fusion Upconversion: Triplet Sensitizers beyond Quantum Dots. MRS Commun. 2019, 9, 924–935.
- (13) Wieghold, S.; Nienhaus, L. Engineering 3D Perovskites for Photon Interconversion Applications. *PLoS One* **2020**, *15*, No. e0230299.
- (14) Huang, Z.; Li, X.; Mahboub, M.; Hanson, K. M.; Nichols, V. M.; Le, H.; Tang, M. L.; Bardeen, C. J. Hybrid Molecule—Nanocrystal Photon Upconversion across the Visible and near-Infrared. *Nano Lett.* **2015**, *15*, 5552–5557.
- (15) Okumura, K.; Mase, K.; Yanai, N.; Kimizuka, N. Employing Core-Shell Quantum Dots as Triplet Sensitizers for Photon Upconversion. *Chem.—Eur. J.* **2016**, 22, 7721–7726.
- (16) Wu, M.; Congreve, D. N.; Wilson, M. W. B.; Jean, J.; Geva, N.; Welborn, M.; Van Voorhis, T.; Bulović, V.; Bawendi, M. G.; Baldo, M. A. Solid-State Infrared-to-Visible Upconversion Sensitized by Colloidal Nanocrystals. *Nat. Photonics* **2016**, *10*, 31–34.
- (17) VanOrman, Z. A.; Bieber, A. S.; Wieghold, S.; Nienhaus, L. Green-to-Blue Triplet Fusion Upconversion Sensitized by Anisotropic CdSe Nanoplatelets. *Chem. Mater.* **2020**, *32*, 4734–4742.
- (18) Eaton, S. W.; Fu, A.; Wong, A. B.; Ning, C.-Z.; Yang, P. Semiconductor Nanowire Lasers. *Nat. Rev. Mater.* **2016**, *1*, 16028.
- (19) Quan, L. N.; Kang, J.; Ning, C.-Z.; Yang, P. Nanowires for Photonics. *Chem. Rev.* **2019**, *119*, 9153–9169.
- (20) Tian, B.; Lieber, C. M. Nanowired Bioelectric Interfaces. Chem. Rev. 2019, 119, 9136–9152.
- (21) Hochbaum, A. I.; Yang, P. Semiconductor Nanowires for Energy Conversion. *Chem. Rev.* **2010**, *110*, 527–546.
- (22) Zhang, S.-Y.; Regulacio, M. D.; Han, M.-Y. Self-Assembly of Colloidal One-Dimensional Nanocrystals. *Chem. Soc. Rev.* **2014**, 43, 2301–2323
- (23) Joarder, B.; Yanai, N.; Kimizuka, N. Solid-State Photon Upconversion Materials: Structural Integrity and Triplet—Singlet Dual Energy Migration. J. Phys. Chem. Lett. 2018, 9, 4613—4624.
- (24) Lin, T. A.; Perkinson, C. F.; Baldo, M. A. Strategies for High-Performance Solid-State Triplet—Triplet-Annihilation-Based Photon Upconversion. *Adv. Mater.* **2020**, *32*, 1908175.
- (25) Mase, K.; Okumura, K.; Yanai, N.; Kimizuka, N. Triplet Sensitization by Perovskite Nanocrystals for Photon Upconversion. *Chem. Commun.* **2017**, *53*, 8261–8264.
- (26) Huang, Z.; Li, X.; Yip, B. D.; Rubalcava, J. M.; Bardeen, C. J.; Tang, M. L. Nanocrystal Size and Quantum Yield in the Upconversion of Green to Violet Light with CdSe and Anthracene Derivatives. *Chem. Mater.* **2015**, *27*, 7503–7507.
- (27) Gray, V.; Xia, P.; Huang, Z.; Moses, E.; Fast, A.; Fishman, D. A.; Vullev, V. I.; Abrahamsson, M.; Moth-Poulsen, K.; Lee Tang, M. CdS/ZnS Core—Shell Nanocrystal Photosensitizers for Visible to UV Upconversion. *Chem. Sci.* **2017**, *8*, 5488—5496.

- (28) Okumura, K.; Yanai, N.; Kimizuka, N. Visible-to-UV Photon Upconversion Sensitized by Lead Halide Perovskite Nanocrystals. *Chem. Lett.* **2019**, *48*, 1347–1350.
- (29) He, S.; Luo, X.; Liu, X.; Li, Y.; Wu, K. Visible-to-Ultraviolet Upconversion Efficiency above 10% Sensitized by Quantum-Confined Perovskite Nanocrystals. *J. Phys. Chem. Lett.* **2019**, *10*, 5036–5040.
- (30) Xia, P.; Raulerson, E. K.; Coleman, D.; Gerke, C. S.; Mangolini, L.; Tang, M. L.; Roberts, S. T. Achieving Spin-Triplet Exciton Transfer between Silicon and Molecular Acceptors for Photon Upconversion. *Nat. Chem.* **2020**, *12*, 137–144.
- (31) Lai, R.; Wu, K. Red-to-Blue Photon Upconversion Based on a Triplet Energy Transfer Process Not Retarded but Enabled by Shell-Coated Quantum Dots. J. Chem. Phys. 2020, 153, 114701.
- (32) Mahboub, M.; Maghsoudiganjeh, H.; Pham, A. M.; Huang, Z.; Tang, M. L. Triplet Energy Transfer from PbS(Se) Nanocrystals to Rubrene: The Relationship between the Upconversion Quantum Yield and Size. *Adv. Funct. Mater.* **2016**, *26*, 6091–6097.
- (33) Luo, X.; Lai, R.; Li, Y.; Han, Y.; Liang, G.; Liu, X.; Ding, T.; Wang, J.; Wu, K. Triplet Energy Transfer from CsPbBr3 Nanocrystals Enabled by Quantum Confinement. *J. Am. Chem. Soc.* **2019**, *141*, 4186–4190.
- (34) Peng, Z. A.; Peng, X. Formation of High-Quality CdTe, CdSe, and CdS Nanocrystals Using CdO as Precursor. *J. Am. Chem. Soc.* **2001**, *123*, 183–184.
- (35) He, S.; Lai, R.; Jiang, Q.; Han, Y.; Luo, X.; Tian, Y.; Liu, X.; Wu, K. Engineering Sensitized Photon Upconversion Efficiency via Nanocrystal Wavefunction and Molecular Geometry. *Angew. Chem., Int. Ed.* **2020**, *59*, 17726–17731.
- (36) Mahboub, M.; Huang, Z.; Tang, M. L. Efficient Infrared-to-Visible Upconversion with Subsolar Irradiance. *Nano Lett.* **2016**, *16*, 7169–7175.
- (37) Kagan, C. R.; Murray, C. B.; Nirmal, M.; Bawendi, M. G. Electronic Energy Transfer in CdSe Quantum Dot Solids. *Phys. Rev. Lett.* **1996**, *76*, 1517–1520.
- (38) Chou, K.; Dennis, A. Förster Resonance Energy Transfer between Quantum Dot Donors and Quantum Dot Acceptors. *Sensors* **2015**, *15*, 13288–13325.
- (39) Huang, Z.; Tang, M. L. Designing Transmitter Ligands That Mediate Energy Transfer between Semiconductor Nanocrystals and Molecules. *J. Am. Chem. Soc.* **2017**, *139*, 9412–9418.
- (40) Dexter, D. L. A Theory of Sensitized Luminescence in Solids. *J. Chem. Phys.* **1953**, *21*, 836–850.
- (41) Zhou, Y.; Castellano, F. N.; Schmidt, T. W.; Hanson, K. On the Quantum Yield of Photon Upconversion via Triplet—Triplet Annihilation. *ACS Energy Lett.* **2020**, *5*, 2322–2326.
- (42) Rigsby, E. M.; Miyashita, T.; Jaimes, P.; Fishman, D. A.; Tang, M. L. On the Size-Dependence of CdSe Nanocrystals for Photon Upconversion with Anthracene. *J. Chem. Phys.* **2020**, *153*, 114702.
- (43) Kriegel, I.; Scotognella, F.; Soavi, G.; Brescia, R.; Rodríguez-Fernández, J.; Feldmann, J.; Lanzani, G.; Tassone, F. Delayed Electron Relaxation in CdTe Nanorods Studied by Spectral Analysis of the Ultrafast Transient Absorption. *Chem. Phys.* **2016**, *471*, 39–45.
- (44) Klimov, V. I. Optical Nonlinearities and Ultrafast Carrier Dynamics in Semiconductor Nanocrystals. *J. Phys. Chem. B* **2000**, *104*, 6112–6123.
- (45) Mongin, C.; Garakyaraghi, S.; Razgoniaeva, N.; Zamkov, M.; Castellano, F. N. Direct Observation of Triplet Energy Transfer from Semiconductor Nanocrystals. *Science* **2016**, *351*, 369–372.
- (46) Monguzzi, A.; Mezyk, J.; Scotognella, F.; Tubino, R.; Meinardi, F. Upconversion-Induced Fluorescence in Multicomponent Systems: Steady-State Excitation Power Threshold. *Phys. Rev. B* **2008**, *78*, 195112.
- (47) Ronchi, A.; Brazzo, P.; Sassi, M.; Beverina, L.; Pedrini, J.; Meinardi, F.; Monguzzi, A. Triplet-Triplet Annihilation Based Photon up-Conversion in Hybrid Molecule—semiconductor Nanocrystal Systems. *Phys. Chem. Chem. Phys.* **2019**, *21*, 12353–12359.
- (48) Cheng, Y. Y.; Khoury, T.; Clady, R. G. C. R.; Tayebjee, M. J. Y.; Ekins-Daukes, N. J.; Crossley, M. J.; Schmidt, T. W. On the Efficiency

Limit of Triplet-Triplet Annihilation for Photochemical Upconversion. *Phys. Chem. Chem. Phys.* **2009**, *12*, 66–71.

- (49) Schmidt, T. W.; Castellano, F. N. Photochemical Upconversion: The Primacy of Kinetics. *J. Phys. Chem. Lett.* **2014**, *5*, 4062–4072.
- (50) De Roo, J.; Huang, Z.; Schuster, N. J.; Hamachi, L. S.; Congreve, D. N.; Xu, Z.; Xia, P.; Fishman, D. A.; Lian, T.; Owen, J. S.; Tang, M. L. Anthracene Diphosphate Ligands for CdSe Quantum Dots; Molecular Design for Efficient Upconversion. *Chem. Mater.* **2020**, 32, 1461–1466.
- (51) Huang, Z.; Simpson, D. E.; Mahboub, M.; Li, X.; Tang, M. L. Ligand Enhanced Upconversion of Near-Infrared Photons with Nanocrystal Light Absorbers. *Chem. Sci.* **2016**, *7*, 4101–4104.
- (52) Zhang, J.; Kouno, H.; Yanai, N.; Eguchi, D.; Nakagawa, T.; Kimizuka, N.; Teranishi, T.; Sakamoto, M. Number of Surface-Attached Acceptors on a Quantum Dot Impacts Energy Transfer and Photon Upconversion Efficiencies. ACS Photonics 2020, 7, 1876–1884
- (53) Wieghold, S.; Bieber, A. S.; VanOrman, Z. A.; Nienhaus, L. Influence of Triplet Diffusion on Lead Halide Perovskite-Sensitized Solid-State Upconversion. *J. Phys. Chem. Lett.* **2019**, *10*, 3806–3811.